ZnO/CdS/$CuGaSe_2$ SOLAR CELLS – ABSORBER AND DEVICE PROPERTIES

M. Rusu*

Hahn-Meitner-Institut Berlin, Department of Solar Energy SE2, Glienickerstr. 100, D-14109 Berlin, Germany
State University of Moldova, Department of Physics, A. Mateevici str. 60, MD-2009 Chisinau, Republic of Moldova
E-mail: rusu@hmi.de

Abstract

For solar cells based on $CuGaSe_2$ (CGSe) polycrystalline thin films, a novel chemical close-spaced vapor transport technique is used to deposit CGSe absorber. Film characterisation including X-ray diffraction measurements, scanning electron microscopy observations, X-ray fluorescence and elastic recoil detection analysis has been carried out. Optical measurements were performed to monitor the changes in the CGSe band gap as a function of composition. These results are used for a discussion of the behaviour of the ZnO/CdS/$CuGaSe_2$ solar cell photovoltaic parameters as well as of the current transport. For the first time, a thermally activated Shockley-Read-Hall recombination mechanism is observed for the CGSe-based solar cells in a large temperature region.

1. Introduction

I-III-VI_2 chalcopyrites have demonstrated high photovoltaic potential. A conversion efficiency of 19.5% [1] was achieved on solar cells based on Cu(In,Ga)Se_2 thin films with a band gap of about 1.12 eV. Now, investigation efforts focus on the development of a suitable high band gap partner for the top cell in a tandem solar cell structure. From this point of view, $CuGaSe_2$ (CGSe) with a band gap of 1.68 eV represents a promising candidate. Additionally, CGSe-based solar cells promise interesting advantages for module implementation, related to the high open-circuit voltages theoretically obtainable. It is worth mentioning that solar cells from CGSe single crystals grown by chemical vapor transport (CVT) in a closed system have reached efficiencies of 9.7% [2], while 10.2% [3] efficient solar cells were prepared by using polycrystalline CGSe thin films grown by physical vapor deposition (PVD). The latter method, however, uses high temperatures (above 1000°C) for the evaporation of the I- and III-group metals. Alternatively, we have implemented a novel efficient chemical close-spaced vapor transport (CCSVT) technique [4] for chalcopyrites deposition at moderate source and substrate temperatures, i.e. 550°C-580°C and 450°C-530°C respectively. With the newly developed CCSVT technique, single phase CGSe thin films were deposited at high deposition rates on areas as large as 10 x 10 cm^2 [5]. Recently, the ZnO/CdS/$CuGaSe_2$ devices reached an efficiency of up to 8.7% with our CCSVT process [5] that allows a fine tuning of the CGSe composition and electronic properties.

In this contribution, namely the new CCSVT method is used for the deposition of CGSe thin films for fundamental investigations and preparation of solar cells. The fine tuning of the CGSe absorber composition which results in a precise control of the absorber properties and

*Corresponding author. Tel.: +49-30-8062-2604; fax: +49-30-8062-3199.

solar cell device parameters is presented. The transport mechanism in the ZnO/CdS/$CuGaSe_2$ heterostructure is analysed and an energetic band diagram proposed. Based on this diagram, we explain the behaviour of the solar cells photovoltaic parameters with respect to the absorber composition.

2. Experiment

2.1 Absorber and device preparation

Usually, high quality I-III-VI_2 absorber thin films are prepared by PVD [6, 7] or molecular beam deposition [8]. These techniques require high temperatures for the source material evaporation (above 1000°C). However, thin film preparation expenses can be significantly decreased by taking advantages of the (i) CVT [2, 9] and close-spaced vapor transport (CSVT) [10-12] approaches, namely, fast volatilisation of source materials by reaction with halogens such as molecular I_2, Br_2, Cl_2 or HCl to gaseous halogenids which occurs at moderate temperatures, and (ii) by using III-VI compounds exhibiting low sublimation temperatures in combination with copper-selenides and -sulphides [13, 14], and also (iii) by employing advantages of the rapid thermal processing (RTP) [15]: thermal annealing of the metal precursors deposited on large areas. Taking into account these advantages, we have developed a new chemical close-spaced vapor transport (CCSVT) technique [4] for the deposition of high-quality binary and multinary compounds.

CSVT using iodine as a transport agent has been reported as a feasible technique for the growth of thin films of $CuInSe_2$ and $Cu(In,Ga)Se_2$ [10-12]. However, experiments were carried out in systems with small working areas (reactor diameters of 20-25 mm) [10, 12] and no data was reported on source stability. This was pointed out as a critical issue in the case of CGSe growth [9] as the volatilisation of the ternary compound by I_2/H_2 in the CVT system occurs non-stoichiometrically, leading to the formation of a Cu_2Se secondary phase on the source material. A satisfactory phase and compositional stability was, however, reported for the use of Ga_2Se_3 and Cu_2Se sources. A high stability of the Ga_2Se_3 source has been demonstrated in our experiments with Ga_2Se_3 deposition on different substrates by CCSVT [16]. Thus, III-VI and I-VI compounds provide stable material sources suitable for the sequential deposition of multinary-compound thin films employing only the CCSVT system. However, as was commented above, chalcopyrites could also be prepared by annealing of evaporated, sputtered, or chemically deposited metallic films, and metallic foils in vapors of III-VI compounds or in their reaction products with I_2, Cl_2 or HCl. Namely this latter simplest way has been chosen for the CGSe thin film preparation: thermal and chemical annealing of Cu layers in the CCSVT reactor employing Ga_2Se_3 as a source material.

A schematic drawing of the CCSVT system is shown in Fig. 1. The CCSVT reactor consists of a graphite reaction cell placed in a quartz box, which has an inlet tube for the gaseous transport agents (I_2, HCl) used for volatilisation of the Ga_2Se_3 source material. A spacer is used for adjustment of the distance between the source drawer and the substrate holder ($D_{source\text{-}substrate}$), where substrates up to 10 x 10 cm^2 can be mounted. The source material in the form of fine grained powder synthesized from 6N pure elements fills the source drawer, which allows an easy refilling. The complete CCSVT quartz box is placed in a quartz tube, which can be evacuated or filled with H_2. The reactor pressure ($p_{reactor}$) can be varied from 10^{-2} mbar up to 1000 mbar. Collectively arranged infrared units (12 infrared lamps-1000 W each) are used as heaters for the source drawer and the substrates. The temperatures can be set independently and are controlled by thermocouples at the source and substrate side.

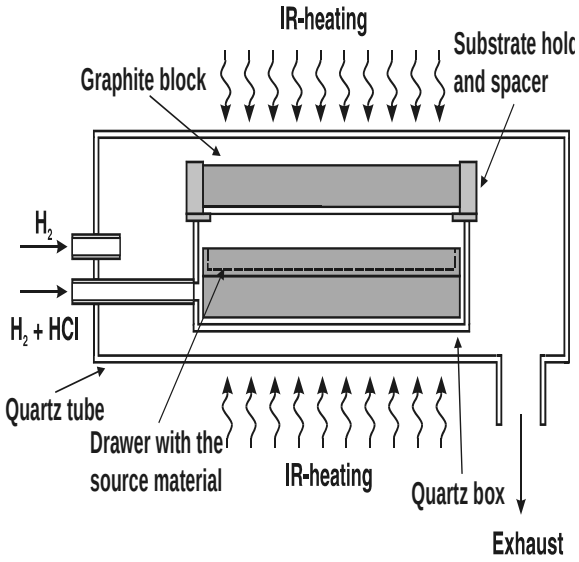


Fig. 1. Schematic drawing of the CCSVT apparatus.

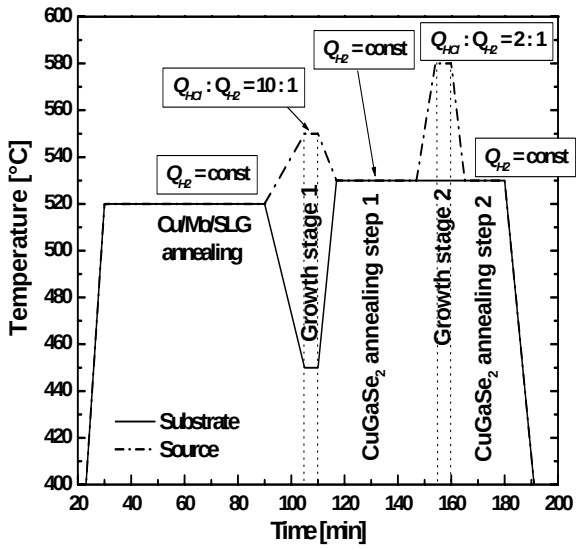


Fig. 2. Source and substrate temperature vs. process time including all steps during the $CuGaSe_2$ thin film growth by CCSVT. Q_{H2} and Q_{HCl} are H_2 and HCl quantities, respectively.

Gaseous HCl diluted in H_2 is used as a transport agent, while additional hydrogen serves as an ambience in the quartz tube, which surrounds the reaction cell. The HCl and H_2 gas quantities, Q_{HCl} and Q_{H2} respectively, are externally controlled by mass-flow controllers. Substrates consisting of 250 nm thick Cu films evaporated on clean and Mo-coated (Mo thickness of ≈ 750 nm) soda lime glass (SLG) were used for CGSe growth. All steps of the CGSe preparation process are shown in Fig. 2. In the first step, the source temperature (T_{source}) and the substrate temperature ($T_{substrate}$) are increased simultaneously up to 520°C at a constant hydrogen flow. At this substrate annealing temperature ($T_{substrate\text{-}a}$) during a substrate annealing time (t_s), the Cu surface of the Cu/Mo/SLG structure is in-situ cleaned from copper oxides by reduction with hydrogen. This step is also used for the preliminary Na diffusion from the SLG substrate. Subsequently, the process parameters are adjusted to the optimum Ga_2Se_3 deposition conditions [16]: T_{source} = 550°C, $T_{substrate}$ = 450°C, $p_{reactor}$ = 800 mbar, Q_{HCl}/Q_{H2} = 10/1 at $D_{source\text{-}substrate}$ = 8 mm, the latter being fixed in advance. Chemical reactions between solid Ga_2Se_3 and gaseous HCl and H_2 occur. In equilibrium, at high HCl to H_2 ratio (HCl: H_2>1 Mol: 50 Mol), the corresponding reaction is expressed by

$$2\ Ga_2Se_3\,(s) + 7\ HCl\,(g) + 2.5\ H_2\,(g) \leftrightarrow 2\ GaCl\,(g) + GaCl_2\,(g) + GaCl_3\,(g) + 6\ H_2Se\,(g), \quad (1)$$

where g = gaseous, s = solid.

The Cu from the substrate reacts with the gaseous compounds GaCl, $GaCl_2$, $GaCl_3$ and H_2Se, leading to the qrowth of CGSe. Single phase CGSe thin films were prepared with a growth rate of 230-240 nm/min using only this first preparation stage, hereafter referred to as 'growth stage 1' (GS-1), by adjusting the corresponding deposition time (t_{g1}). However, sometimes, probably because of incomplete reactions at a high deposition rate, the deposited CGSe contained $Cu_{2-x}Se$ phases. Therefore, in further experiments, t_{g1} was adjusted for the preparation of Cu-rich CGSe thin films. After stopping the HCl provision, this step was then

followed by annealing the CGSe thin film at an annealing temperature T_{a1} of 530°C – the melting point of CuSe [17]. Liquid CuSe together with $Cu_{2-x}Se$ species, which are in quasi-liquid state at this temperature [18] serve as solvents for the Ga-Se phase. The CGSe growth is aided by the liquid Cu-Se phase and the crystalline quality of the growing CGSe grains is improved. Maintaining a constant $p_{reactor}$ and $T_{substrate}$, the source temperature is then increased up to 580°C and Q_{HCl}/Q_{H2}–ratio is fixed at ~ 2/1. Owing to the reduced HCl content in the H_2 flux and, correspondingly, lower, GaCl, $GaCl_2$, $GaCl_3$ and H_2Se concentrations, and also because of a smaller temperature difference between the source and the substrate, the CGSe growth rate is significantly reduced. In this way, fine tuning of the CGSe layer thickness and composition is realised in the second growth stage – GS-2 (see section 3). Finally, 'CGSe annealing step 2' is used for the layer homogenisation in the presence of H_2 ambience only. After the last step, the reactor is cooled down.

The absorber films are deposited on uncoated SLG for optical characterisation and on Mo/SLG for morphology, structural and compositional analysis as well as for devices. The typical thickness of the absorber films ranges from 1.6 μm to 1.9 μm. The [Ga]/[Cu] ratio of the thin films is adjusted within the range of 0.9-1.3. Solar cell devices consisting of ZnO: Ga/i-ZnO/CdS/CGSe/Mo/SLG structures were processed from as-grown CGSe films. A 50-nm-thick CdS buffer layer was prepared by chemical bath deposition (CBD) at 60°C. The sputtered window layer consists of a 90 nm intrinsic and of a 400 nm highly Ga-doped ZnO. Ni/Al grids were evaporated by e-beam to provide the front contacts.

2.2 Characterisation techniques

The CGSe films were characterised by means of X-ray diffraction (XRD) with a Bruker D8 diffractometer in order to identify crystallographic phases. The phase analysis of the CGSe layer surface was performed by grazing incidence measurements (GI-XRD). The cross-section and surface morphology of the thin films were investigated by scanning electron microscopy (SEM), using a commercial Leica/Zeiss LEO430 microscope. Compositional analysis and thickness determination of the CGSe/Mo/SLG layers was attained by highly precise X-ray fluorescence analysis (XRF) using a Philips MagiXPro PW2400 spectrometer. Elastic recoil detection analysis (ERDA) technique using 230 MeV ^{129}Xe ions as projectiles was applied at the Ionenstrahllabor (ISL) of the Hahn-Meitner-Institut to obtain the absolute atomic concentrations as a function of film depth. Details about the ERDA principle and the experimental setup can be found in Ref. [19].

Optical transmission and reflection measurements are carried out at 300 K on CGSe films deposited on SLG substrates using a Cary 500 spectrometer (Varian) in combination with an integrating sphere in order to collect also the scattered light. Analysis of the reflection and transmission data is used for the evaluation of the absorption coefficient (α), as well as energy transitions (E_0) at the CGSe fundamental absorption edge.

The photovoltaic (PV) parameters - power conversion efficiency (η), fill factor (FF), open circuit voltage (V_{oc}), short-circuit current density (J_{sc}) - are determined from J-V measurements performed under standard test conditions (AM1.5; 100 mW/cm^2; 25°C).

Measurements of the current-voltage characteristics as a function of temperature (JV-T) and illumination are performed in an evacuated home made N_2-cooled cryostat using a source measure unit in four-point configuration. The samples are illuminated by an ELH-type halogen lamp. A set of neutral density filters serve for the light intensity adjusting.

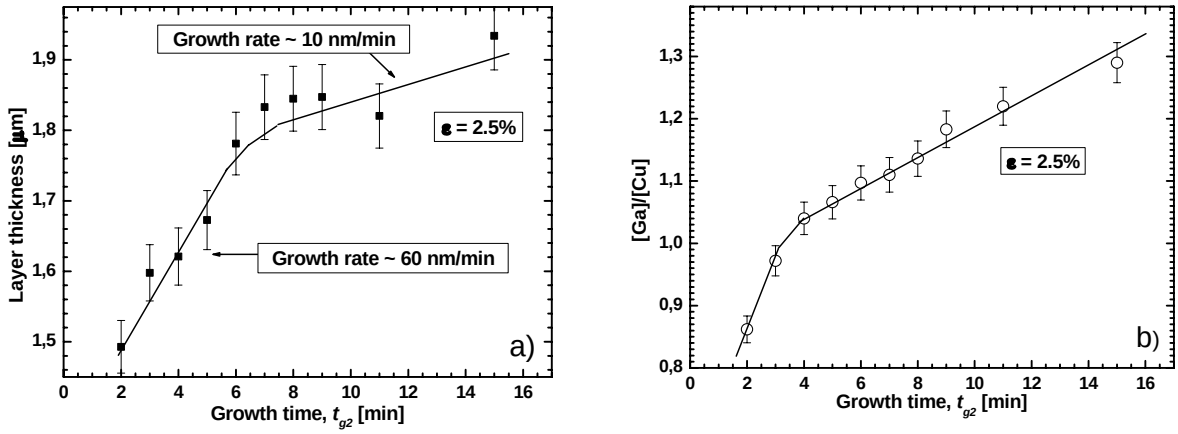


Fig. 3. $CuGaSe_2$ (a) layer thickness and (b) [Ga]/[Cu] ratio vs. growth time t_{g2} during the second stage of the CCSVT process.

3. Results and discussion

3.1 CGSe growth and characterisation

As mentioned in §2.1, CGSe films grown in the stage GS-1 result in CGSe films containing $Cu_{2-x}Se$ secondary phases. A second growth stage was implemented to dissolve the $Cu_{2-x}Se$ phases and to adjust the CGSe composition and electronic properties for subsequent solar cell preparation. XRF data including layer composition and thickness combined with XRD spectra were used to monitor the influence of the growth stage GS-2 on the film parameters. Fig. 3-a and Fig. 3-b illustrate the layer thickness and [Ga]/[Cu] ratio as a function of the deposition time t_{g2}. As can be seen, these parameters are controlled by the CCSVT process within fluctuation of ~ 2.5%. In the first minutes of the GS-2 the CGSe layers continue to grow with a growth rate of ≈ 60 nm/min due to the transformation of the remained $Cu_{2-x}Se$ phase after the growth stage GS-1 into CGSe (see XRD patterns in Fig. 4). After ~ 3 min of the GS-2, Cu_2Se is not further detected by XRD and only those peaks corresponding to tetragonal (chalcopyrite) crystal structure are recorded in the XRD spectrum. For the CGSe layers prepared with [Ga]/[Cu] ratios of up to 1.29 the Ga_2Se_3 phase is not observed neither in the CGSe bulk (Fig. 4) nor on the layer surface as inferred from GI-XRD (not shown). Only peaks corresponding to CGSe are found in the GI-XRD measurements performed at incident angles of 1° and 0.3°. Once CGSe stoichiometry is achieved, the [Ga]/[Cu] ratio continues to increase linearly with t_{g2}, but with a smaller slope (see Fig. 3-b). A further increase of the CGSe thickness is limited to ≈ 10 nm/min.

The surface morphology and cross-section images of CGSe films are presented in Figs. 5-a, -b, respectively. The films posseses a rough surface, with triangular-like grain shapes having sizes of up to 2 μm. It was reported that such a morphology is typical for of layers grown under Cu-rich conditions [20]. Cross-sectional SEM-images indicate that the films are densely packed and, in some places, tend to grow in a columnar structure.

By means of the ERDA technique, the depth profiling of the elements concentration from an overall Ga-rich grown CGSe film was extracted. The relative amount of the elements vs. distance from the film surface is plotted in Fig. 6. The bulk concentration of the elements Cu, Ga, and Se are nearly constant throughout the film, with only slight Se gradient towards the film top surface, while the CGSe surface side is Ga- and Cu-poor, and Se-rich. Carbon and oxygen were detected at a concentration below 0.5 at.% and an insignificant amount of H (< 0.05 at.%) was also found. Na and Cl have been found as major contaminants. The Cl

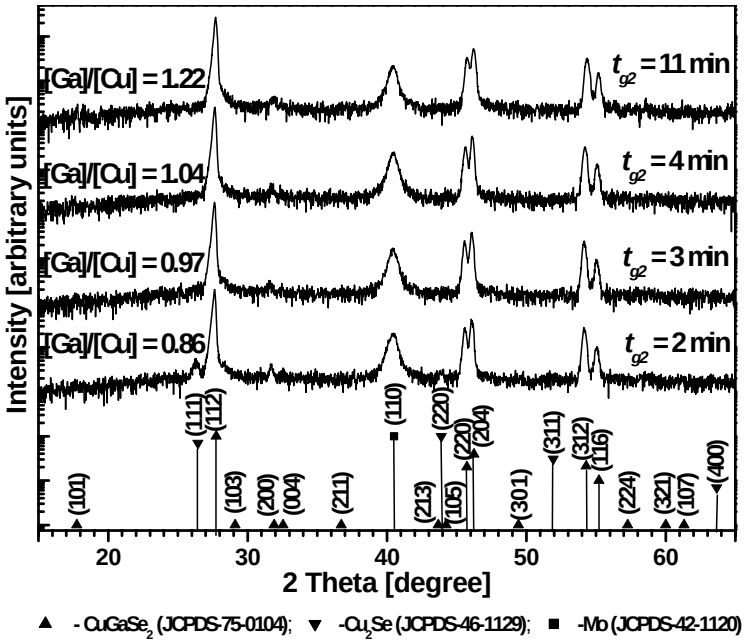


Fig. 4. XRD patterns of the $CuGaSe_2$ thin films grown by CCSVT on Mo/SLG substrates depending on growth time t_{g2} in the second stage. All other process parameters are kept constant, as indicated in Fig. 2. The lines and symbols mark $CuGaSe_2$, Cu_2Se and Mo peak positions according to JCPDS data.

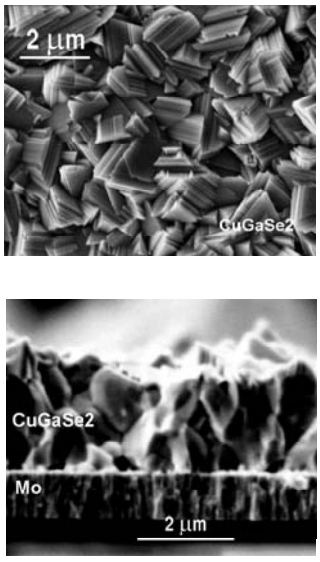


Fig. 5. (a) Top view and (b) cross-section SEM images of a CCSVT-grown $CuGaSe_2$ thin film ([Ga]/[Cu] = 1.11) on Mo/SLG substrate.

concentration decreases gradually with increasing distance from the rear side and becomes undetectable at a distance of ≈ 400 nm from the surface side. Such a Cl concentration behaviour correlates well with the CCSVT process stage peculiarities. Cl is incorporated in the CGSe during the first growth stage when deposition occurs at high HCl concentration (see §2.1). At the second growth stage the Cl concentration is five times lower than at the first one, resulting in Cl incorporation below the ERDA detection limit. The Na presence is due to diffusion from the SLG glass. During the absorber growth and the annealing steps, Na diffuses through the Mo film into the absorber, improving the doping concentration of the Ga-rich absorber. A higher Na amount is found closer to the Mo contact. The Na concentration gradually decreases in the bulk. Thus, the concentration gradient is realised near the rear side.

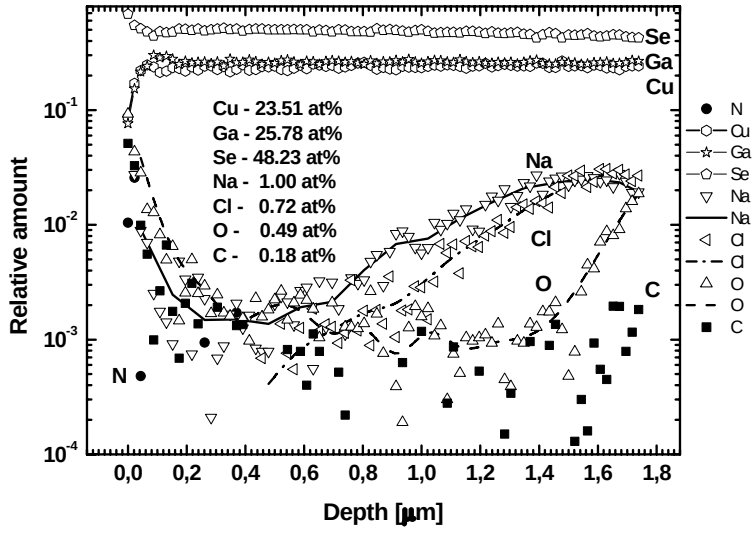


Fig. 6. The ERDA depth-resolved elemental concentrations of the film depicted in Fig. 5. The inset shows the averaged elemental concentrations

On the film surface Na is found with a concentration of 1at.%. However, the CGSe surface state could be essentially changed during the CBD of the CdS-buffer. This will be a subject of our further investigations.

3.2. CGSe optical properties

We investigate the CGSe thin films' optical properties as a function of [Ga]/[Cu] ratio. Special attention is paid to the film composition influence on the CGSe fundamental absorption edge. The structure of the fundamental absorption edge of chalcopyrites is well understood [21]. These crystals are semiconductors with a direct fundamental gap. The valence-band maximum is composed of three nondegenerate states, giving rise to three transitions called $E_0(A)$, $E_0(B)$, and $E_0(C)$ from smaller to larger energy. In a simplified model, $E_0(A)$ and $E_0(B)$ are regarded as a crystal-field-split gap, and the higher energy $E_0(C)$ transition corresponds to the spin-orbit-split gap. Usually, these three transitions are resolved in the CGSe samples [21], which is also the case in the absorption spectra of the CCSVT-grown CGSe thin films. The absorption coefficient of CGSe thin films with defined thickness and composition, i. e. determined [Ga]/[Cu] ratio, has been calculated using equation (2) [22] and by means of optical transmission and reflection data taken at 300K:

$$\alpha = -\frac{1}{t}\ln\left(\frac{\sqrt{(1-R)^4 + 4T^2R^2} - (1-R)^2}{2TR^2}\right), \qquad (2)$$

where α is the absorption coefficient, t is the thickness of the film, T and R are the transmission and reflectance, respectively. The results were plotted as a function of energy of the incident photons for the [Ga]/[Cu] ratio ranging between 0.95 and 1.29 (not shown). The analysis of the absorption coefficient spectra revealed the presence of three optical transitions at the photon energies of approximately 1.67 eV, 1.75 eV, and 1.93 eV. A shift of the absorption edge towards longer wavelengths with increasing [Ga]/[Cu] ratio is observed, as well as a broadening of the CGSe distinct structure corresponding to the three band-to-band transitions described above. The observed broadening of the spectra in Ga-rich CGSe can be explained both by the effect of shrinking of the CGSe crystalline unit cell with increasing Ga content [23] and high doping and compensation on the band structure of semiconductors. The latter effect is described by the model of fluctuating potentials [24]. The $\alpha^2 = f(h\nu)$ curves (Fig. 7-a) were plotted since in the case of allowed direct transitions the absorption coefficient α is expressed as $\alpha(h\nu) = A^*(h\nu - E_g)^{1/2}$ [25], where A^* is a constant and E_g is the corresponding semiconductor band gap, or, in our case, E_g is associated with the three energies $E_0(A)$, $E_0(B)$, and $E_0(C)$ of the CGSe fundamental absorption. Thus, the energies $E_0(A)$, $E_0(B)$, and $E_0(C)$ can be determined as a function of [Ga]/[Cu] ratio by extrapolation of the linear parts of the respective $(\alpha_{1,2,3})^2 = f(h\nu)$ spectra to zero, where α_1, α_2, and α_3 are the absorption coefficient data extracted from the energy range of the corresponding transition from the general $\alpha = f(h\nu)$ spectra. The data are presented in Fig. 7-b. The $E_0(A)$, $E_0(B)$, and $E_0(C)$ values at [Ga]/[Cu] = 1.0 are close to the reported data [26]. All the curves exhibit similar behaviour. Almost constant values are observed up to [Ga]/[Cu] = 1.05, consistent with the results of Mikkelsen [27] that the homogeneity range of chalcopyrite phase extends into the Ga-rich side. The E_0 energies decrease then gradually with [Ga]/[Cu] ratio increase to 1.16. Further increase of the Ga content weakly influences the E_0, consistent with the reported [28] constancy of the lattice parameters in this compositional range.

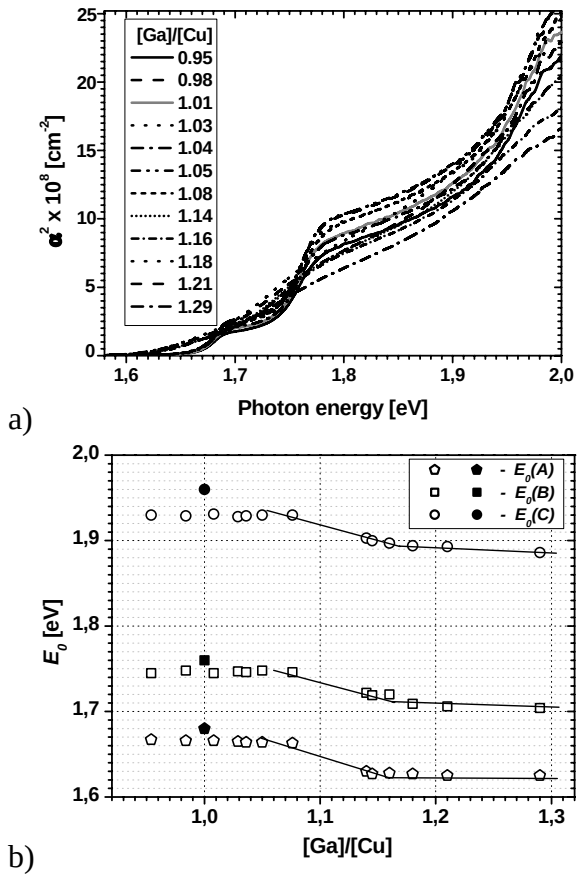


Fig. 7. (a) α^2 versus photon energy for the CCSVT-grown $CuGaSe_2$ thin films with different [Ga]/[Cu] ratio. (b) The evolution of the $E_0(A)$, $E_0(B)$, and $E_0(C)$ energy transitions at the fundamental absorption edge of $CuGaSe_2$ thin films with varying the [Ga]/[Cu] ratio. The open symbols represent the data extracted from the $\alpha^2=f(h\nu)$ curves and the full symbols display the reported values [26].

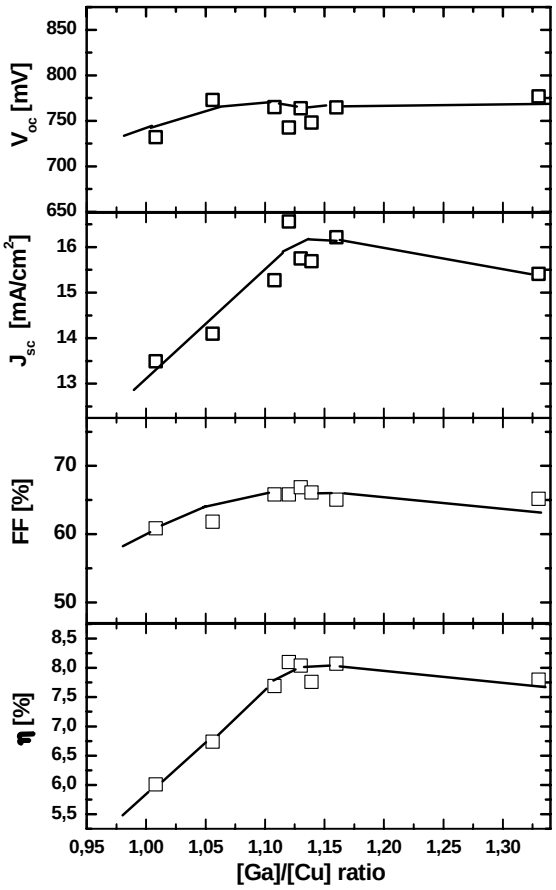


Fig. 8. Photovoltaic parameters of the ZnO/CdS/$CuGaSe_2$ solar cells based on as-grown $CuGaSe_2$ absorbers prepared by the CCSVT technique with varying the [Ga]/[Cu] ratio. No antireflection coating was used. The lines depict guides to the eye.

3.3 ZnO/CdS/$CuGaSe_2$ device properties

Figure 8 displays the photovoltaic parameters of the ZnO/CdS/$CuGaSe_2$ solar cells under AM1.5 conditions [29]. The device reach a maximum total area efficiency of 8.1% at a [Ga]/[Cu] = 1.12. Afterwards it decreases monotonically with increase of Ga content. As can be seen, the η behaviour with the composition is mainly governed by the short-circuit current since V_{oc} and FF depend weakly on the [Ga]/[Cu] ratio of the CGSe films in the investigated compositional range.

The best device was chosen for the investigation of the transport mechanism in the ZnO/CdS/$CuGaSe_2$ solar cells with CCSVT-grown CGSe. Under AM1.5 conditions (100 mW/cm^2) this device shows the following parameters: V_{oc} = 743 mV, J_{sc} = 17.7 mA/cm^2, FF = 65.8%, and an efficiency of 8.7% (active area, no antireflection coating). The high value of the short-circuit current density is confirmed by quantum efficiency measurements [5].

The dark and illuminated *JV-T* curves were analyzed following the model proposed for

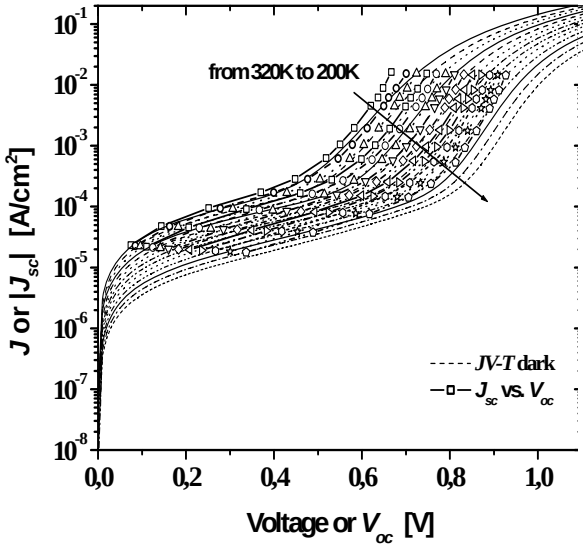


Fig. 9. Temperature-dependent *JV* curves and J_{sc} vs. V_{oc} plots measured with the temperature step of 10 K on a ZnO/CdS/$CuGaSe_2$ solar cell based on CCSVT-grown Ga-rich $CuGaSe_2$ with [Ga]/[Cu] = 1.12 showing an efficiency of 8.7% under AM1.5 conditions.

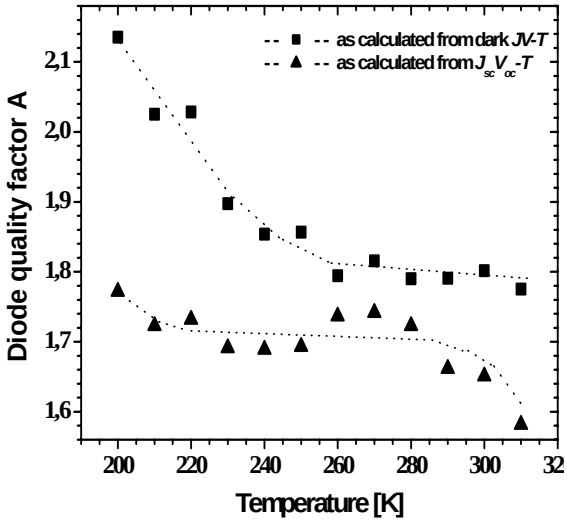


Fig. 10. Temperature dependence of the diode quality factors of the ZnO/CdS/$CuGaSe_2$ device shown in Fig. 9 with the data extracted from the dark *JV* curves and J_{sc} versus V_{oc} plots. The dashed lines are guides to the eye.

the chalcopyrite solar cells [31]. The forward current density J of the heterojunction is described by

$$J = J_0 \exp\left(\frac{qV}{AkT}\right) = J_{00} \exp\left(\frac{-E_a}{AkT}\right) \exp\left(\frac{qV}{AkT}\right), \tag{3}$$

where kT/q is the thermal voltage, J_{00} is a weakly temperature-dependent prefactor, and E_a is the activation energy of the recombination. By reorganising Eq. (3) to the relationship

$$A\ln(J_0) = -\frac{E_a}{kT} + A\ln(J_{00}), \tag{4}$$

a refined evaluation of E_a is attained. Thus, a plot of the corrected saturation current density $Aln(J_0)$ versus the inverse temperature $1/T$ should yield a straight line with a slope corresponding to the activation energy E_a. The value of E_a indicates either bulk recombination when $E_a = E_g$, or interface recombination for $E_a < E_g$.

The dark *JV-T* curves and the J_{sc} versus V_{oc} plots from the best solar cell device at different temperatures are shown in Fig. 9. The forward dark and illuminated *JV-T* curves show similar behaviour in the region of lower voltages and some differences at higher ones. The J_{sc} versus V_{oc} plots exhibit an exponential dependence over more than two orders of magnitude in the temperature range 200-320 K making them suitable for analysis.

The temperature dependence of the diode quality factors A is given in Fig. 10. The ideality factor values calculated by using J_{sc} versus V_{oc} plots are below two and vary between 1.6 and 1.8 showing a weak dependence on temperature. In the dark and temperature region 260 K - 310 K the diode quality factor is independent of temperature at a value of ~1.8. The

diode quality factor *A* increases slightly above two at a measurement temperature of 200 K. Such behaviour of the diode ideality factor indicates that a thermally activated process is

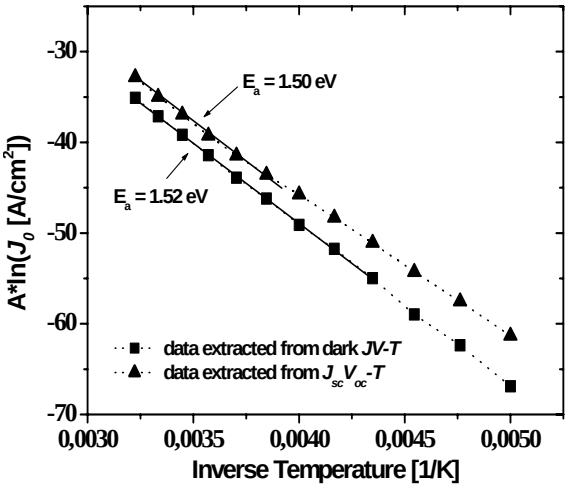


Fig. 11. Arrhenius plot of the saturation current density J_0 corrected by diode quality factors A of the ZnO/CdS/$CuGaSe_2$ solar cell device shown in Fig. 9. The solid lines show the fits to Eq. (4).

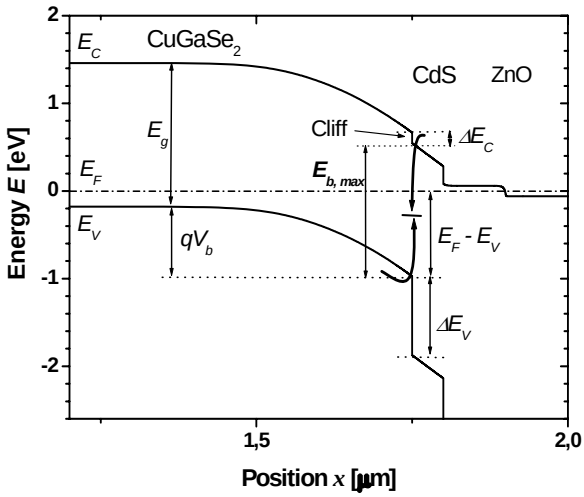


Fig. 12. Equilibrium band diagram of a $CuGaSe_2$/CdS/ZnO heterostructure simulated by the SCAPS program [36]. The quantities E_c, E_v, and E_F denote the conduction band, valence band, and the Fermi energy, respectively; qV_b is the band bending in the absorber material; $\Delta E_c/\Delta E_v$ are the conduction/valence band offsets between $CuGaSe_2$ and CdS. $E_{b,\,max}$ denotes the maximum barrier for interface recombination.

dominant in the recombination process of the charge carriers in the ZnO/CdS/CGSe solar cells under consideration. Tunnelling contribution becomes competitive only at temperatures below 200 K. A thermally activated process, as it is described above, is for the first time observed as the dominant recombination mechanism in CGSe-based solar cells in such a large temperature region. So far tunnelling enhanced recombination has always been reported as dominant [31]. This conclusion is also supported by the J_0 dependence on the inverse temperature (not shown). Both J_0 data extracted from dark and illuminated curves show linear dependences on 1/T, which confirms thermally activated recombination to be the dominant transport mechanism over the full temperature range investigated.

The activation energy of the recombination is determined from the modified Arrhenius graphs of $Aln(J_0)$ *vs.* $1/T$, shown in Fig. 11, where the saturation currents are obtained from the analysis of the dark *JV* characteristics and the J_{sc} versus V_{oc} plots. The slope of the Arrhenius plot, with extracted A and J_0 data from J_{sc} *vs.* V_{oc} curves, yield an activation energy of 1.50 eV. The analysis of the dark measurement results gives an activation energy of 1.52 eV. Thus, the recombination energy E_a = 1.50-1.52 eV is below the E_{gCGSe} = 1.68 eV. We conclude therefore that the dominant recombination process takes place at the CdS/CGSe interface. Moreover, the fact that the diode quality factor values are below two and independent of temperature in a large temperature region, allows us to conclude that the recombination is described by the classical Shockley-Read-Hall recombination model [32] with a single dominant recombination center. This recombination center is situated at the CGSe/CdS interface and lies within a range of energetically distributed defects. The observed transport features of the ZnO/CdS/$CuGaSe_2$ heterostructures investigated are explained on the basis of the band diagram proposed in Fig. 12. The diagram is based on previously reported data [33, 34] and our

experimental data. The CGSe absorber band gap energy of 1.64 eV of the cell under investigation is determined from the $E_0(A) = f$([Ga]/[Cu]) plot in Fig. 7-b, considering $E_0(A)$ as the energy of the lowest CGSe band gap. We assume the valence band offset ΔE_v = 0.90 eV determined by Nadenau et al. [33] for the band alignments at the $CuGaSe_2$/CdS interface with CdS prepared by CBD as in our case. This assumption is also supported by the fact that for $Cu(In,Ga)Se_2$ compounds the energetic distance between the valence band maximum and the Fermi-level remains nearly constant, independent of the Ga content [34]. In addition valence band offsets for the $Cu(In,Ga)Se_2$ and $CuGaSe_2$ thin films with CdS buffer are considered similar [35]. With the above mentioned data, the CdS bulk band gap E_{gCdS} = 2.42 eV and the formula $\Delta E_c = E_{gCdS} - E_{gCuGaSe2} - \Delta E_v$, we calculate a conduction band offset ΔE_c = - 0.12 eV. The activation energy of recombination calculated by the expression $E_a = E_{gCuGaSe2} - \Delta E_c$ is 1.52 eV, E_a corresponding to the maximum barrier $E_{b,max}$ for interface recombination. Thus, we found a perfect correlation between the calculated recombination energy using the band diagram in Fig. 12 and the experimentally found value with the data from the *JV-T* analysis.

With the help of the model in Fig. 12 we explain the J_{sc} and V_{oc} behaviour in Fig. 8. Assuming that the energies ΔE_v and $E_F - E_v$ are independent on the CGSe composition, as discussed above, we expect V_{oc} to be independent of the [Ga]/[Cu] ratio. For this to occur, only the height of the cliff in the conduction band, i. e. ΔE_c, will be influenced by the absorber band gap. For [Ga]/[Cu] < 1.16, the CGSe band gap decreases with a Ga increase to up to 1.63 eV, remaining almost constant for [Ga]/[Cu] ≥ 1.16 (see Fig. 7-b). At the same time $|\Delta E_c|$ decreases to 0.11 eV. Consequently, the carriers' recombination rate at the CGSe/CdS interface should decrease with the [Ga]/[Cu] ratio of the absorber and a rise in J_{sc} should be registered. Such a behaviour of J_{sc} is seen in Fig. 8. The decrease in the short circuit current observed for [Ga]/[Cu] ratios higher than 1.16 is explained by a perturbation of the CGSe bands in highly Ga-rich films. A further refinement of the proposed band diagram requires photoemission measurements, which are in progress.

4. Conclusion

Single phase $CuGaSe_2$ thin films were prepared with a growth rate of up to 240 nm/min on clean and Mo-coated SLG substrates on areas as large as 10 x 10 cm^2 by a novel CCSVT technique. A fine tuning of the CGSe composition and electronic properties appropriate for solar cell preparation was realised. We have shown that the optical $CuGaSe_2$ properties can be tuned by varying the material composition. The data obtained from the CGSe thin film absorption spectra, particularly the CGSe band gap as a function of the [Ga]/[Cu] ratio, are used in a proposed ZnO/CdS/$CuGaSe_2$ band diagram and the behaviour of the device photovoltaic parameters is discussed as a function of composition. The transport mechanism in the ZnO/CdS/$CuGaSe_2$ heterostructures has been investigated and a thermally activated Shockley-Read-Hall recombination via a single dominant recombination center was identified in a large temperature region for CGSe-based solar cells for the fist time. The best conditions for the preparation of solar cells based on CCSVT-grown CGSe absorber have been found.

Acknowledgements

The author thanks M.Ch Lux-Steiner, Th. Schedel-Niedrig and R. Klenk for discussions and all the colleagues who assisted this work. This work is supported by the German Ministry of Research BMWi (No. 0329740B).

References

[1] M.A. Contreras, K. Ramanathan, J. AbuShama, F. Hasoon, D.L. Young, B. Egaas, and R. Noufi, Prog. Photovolt: Res. Appl., 13, 209, (2005).
[2] M. Saad, H. Riazi, E. Bucher, M.Ch. Lux-Steiner, Appl. Phys. A, 62, 181, (1996).
[3] J. AbuShama, S. Johnston, D.L. Young, R. Noufi, Mater. Res. Soc. Symp. Proc. 865, 335, (2005).
[4] German utility model DE 102 08 911.6.
[5] M. Rusu, S. Wiesner, D. Fuertes Marrón, A. Meeder, S. Doka, W. Bohne, S. Lindner, Th. Schedel-Niedrig, Ch. Giesen, M. Heuken, M. Ch. Lux-Steiner, Thin Solid Films 451-452, 556, (2004).
[6] M.A. Contreras, A.M. Gabor, A.L. Tennant, A. Asher, J.R. Tuttle, R. Noufi, Prog. Photovolt., 2, 287, (1994).
[7] V. Nadenau, D. Hariskos, H.W. Schock, J. Appl. Phys., 85, 534, (1999).
[8] M. Nishtani, T. Negamy, M. Terauchi, T. Hirao, Jpn. J. Appl. Phys., 31, 192 (1992).
[9] D. Fischer, N. Meyer, M. Kuczmic, M. Beck, A. Jäger-Waldau, M.Ch. Lux-Steiner, Sol Energy Mater. Sol. Cells, 67, 105, (2001).
[10] K. Guenoun, K. Djessas, G. Masse, J. Appl. Phys., 84-1, 589, (1998).
[11] G. Masse, K. Djessas, Thin Solid Films, 226, 254, (1993).
[12] A. Zouaoui, M. Lachab, M.L. Hidalgo, A. Chaffa, C. Llinares, N. Kesri, Thin Solid Films 339, 10, (1999).
[13] S.Ch. Park, S.H. Kwon, J.S. Song, B.T. Ahn, Sol Energy Mater. Sol. Cells, 50, 43, (1998).
[14] S.Ch. Park, D.Y. Lee, B.T. Ahn, K.H. Yoon, J. Song, Sol. Cells, 69, 99, (2001).
[15] V. Probst, W. Stetter, W. Riedl, H. Vogt, M. Wendl, H. Calwer, S. Zweigart, K.-D. Ufert, B. Freienstein, H. Cerva, F.H. Karg, Thin Solid Films, 387, 262, (2001).
[16] M. Rusu, S. Wiesner, S. Lindner, E. Strub, J. Röhrich, R. Würz, W. Fritsch, W. Bohne, Th. Schedel-Niedrig, M.Ch. Lux-Steiner, Ch. Giesen, M. Heuken, J. Phys.: Condens. Matter, 15, 8185, (2003).
[17] H. Jitsukawa, H. Matsushita, T. Takizawa, J. Crystal Growth, 186, 587, (1998).
[18] R. Klenk, T. Walter, H.W. Schock, D. Cahen, Adv. Mater., 5-2, 114, (1993).
[19] W. Bohne, J. Röhrich, G. Röschert, Nucl. Instr. And Methods B, 136-138, 633, (1998).
[20] D. Fischer, T. Dylla, N. Meyer, M.E. Beck, A. Jäger-Waldau, M.Ch. Lux-Steiner, Thin Solid Films, 387, 63, (2001).
[21] M.I. Alonso, M. Garriga, C.A. Durante Rincon, E. Hernández, M. León, Appl. Phys. A, 74, 659, (2002).
[22] D.K. Schroder, Semiconductor material and device characterisation, John Wiley & Sons Inc., 1990.
[23] D. Fisher, T. Dylla, N. Meyer, M.E. Beck, A. Jäger-Waldau, M.Ch. Lux-Steiner, Thin Solid Films, 387, 63, (2001).
[24] B.J. Shklovskii and A.L. Efros, Electronic properties of doped semiconductors, Berlin, Springer, 1984.
[25] J.I. Pankove, Optical processes in semiconductors, New York: Dover, 1976.
[26] J.L. Shay, B. Tell, H.M. Kasper, L.M. Shiavone Phys. Rev. B, 5, 5003, (1972).
[27] J.C. Mikkelsen, J. Electron Mater., 10, 541, (1981).
[28] M. Klenk, O. Schenker, V. Alberts, U. Probst, E. Bucher, J. Phys. D: Appl. Phys., 36, 2531, (2003).

[29] M. Rusu, S. Doka, C.A. Kaufmann, N. Grigorieva, Th. Schedel-Niedrig, M.Ch. Lux-Steiner, Thin Solid Films, 480-481, 341, (2005).
[30] A. Meeder, D. Fuertes Marrón, A. Rumberg, M.Ch. Lux-Steiner, J. Appl. Phys., 92-6, 3016, (2002).
[31] V. Nadenau, U. Rau, A. Jasenek, H.W. Schock, J. Appl. Phys., 87, 584, (2000).
[32] W. Shockley, W.T. Read, Phys. Rev., 87, 835, (1952).
[33] V. Nadenau, D. Braunger, D. Hariskos, H.W. Schock, Inst. Phys. Conf. Ser., 152, 955, (1998).
[34] V. Nadenau, D. Hariskos, and H.W. Schock. In H.A. Ossenbrink, P. Helm, and H. Ehmann, editors, Proc. 14th Europ. Photovolt. Solar Energy Conf., Bedford, UK, H.S. Stephens & Ass., 1250, (1997).
[35] T. Schulmeyer, R. Kniese, R. Hunger, W. Jaegermann, M. Powalla, A. Klein, Thin Solid Films, 451-452, 420, (2004).
[36] M. Burgelman, P. Nollet, S. Degrave, Thin Solid Films, 361-362, 527, (2000).